

THE OPTICALLY UNBIASED GRB HOST (TOUGH) SURVEY. V. VLT/X-SHOOTER EMISSION-LINE REDSHIFTS FOR *SWIFT* GRBS AT $Z \sim 2$ [†]

THOMAS KRÜHLER¹, DANIELE MALESANI¹, BO MILVANG-JENSEN¹, JOHAN P. U. FYNBO¹, JENS HJORTH¹, PÁLL JAKOBSSON², ANDREW J. LEVAN³,
MARTIN SPARRE¹, NIAL R. TANVIR⁴, DARACH J. WATSON¹

ApJ in press

ABSTRACT

We present simultaneous optical and near-infrared (NIR) spectroscopy of 19 *Swift* GRB host galaxies with VLT/X-shooter with the aim of measuring their redshifts. Galaxies were selected from The Optically Unbiased GRB Host (TOUGH) survey (15 of the 19 galaxies) or because they hosted GRBs without a bright optical afterglow. Here, we provide emission-line redshifts for 13 of the observed galaxies with brightnesses between $F606W > 27$ mag and $R = 22.9$ mag (median $\bar{R} = 24.6$ mag). The median redshift is $\bar{z} = 2.1$ for all, and $\bar{z} = 2.3$ for the TOUGH hosts. Our new data significantly improve the redshift completeness of the TOUGH survey, which now stands at 77% (53 out of 69 GRBs). They furthermore provide accurate redshifts for nine prototypical dark GRBs (e.g., GRB 071021 at $z = 2.452$ and GRB 080207 at $z = 2.086$), which are exemplary of GRBs where redshifts are challenging to obtain via afterglow spectroscopy. This establishes X-shooter spectroscopy as an efficient tool for redshift determination of faint, star-forming, high-redshift galaxies such as GRB hosts. It is hence a further step towards removing the bias in GRB samples that is caused by optically-dark events, and provides the basis for a better understanding of the conditions in which GRBs form. The distribution of column densities as measured from X-ray data ($N_{\text{H,X}}$), for example, is closely related to the darkness of the afterglow and skewed towards low $N_{\text{H,X}}$ values in samples that are dominated by bursts with bright optical afterglows.

Subject headings: gamma-ray burst: general — galaxies: high-redshift — galaxies: distances and redshifts — galaxies: fundamental parameters — surveys — dust, extinction

1. INTRODUCTION

Our understanding of long γ -ray bursts (GRBs, e.g., Piran 2004; Gehrels et al. 2009), their multi-wavelength afterglows, and star-forming host galaxies fundamentally relies on the information about the distance scale to these events. The redshift of a GRB is most robustly obtained via optical/near-infrared (NIR) follow-up observations: afterglow spectroscopy yields a precise redshift measurement through the signature of the host's interstellar medium (ISM) from fine-structure transitions (Prochaska et al. 2006; Vreeswijk et al. 2007) or hydrogen and metal lines (Fynbo et al. 2009b). Also multi-band photometry provides a rough distance scale through the identification of the strong Ly α and Ly-limit breaks (Krühler et al. 2011a).

Redshifts^{6,7} and host data⁸ are publicly available for a large sample of GRBs. The prerequisite of an optical afterglow for redshift measurements, however, causes substantial selection biases due to the phenomenon of optically-dark GRBs (Groot et al. 1998; Djorgovski et al. 2001). A high redshift and significant column densities of dust along the GRB's sight line efficiently suppress afterglow emission in the UV/optical wave-

length bands, where most of the follow-up observations and redshift measurements are performed (e.g., Jakobsson et al. 2004).

This leads to strong selection effects, which arguably play a crucial role when using GRBs as tools, in the distribution of metallicities of GRB damped Ly α absorbers (DLAs, Prochaska et al. 2009), the dust characteristics of GRB sightlines (Greiner et al. 2011; Zafar et al. 2011) as well as the metallicity, luminosity, mass-distribution and Ly α -emission of long GRB hosts (Krühler et al. 2011b; Milvang-Jensen et al. 2012).

A different route to redshift measurements for GRBs without an optical afterglow exists through an association between burst and its host galaxy and subsequent galaxy spectroscopy. This requires GRB positions with an uncertainty of at most few arcseconds. In the absence of optical/NIR afterglows, those positions were previously obtained via radio/sub-mm or X-ray observations (e.g., Djorgovski et al. 2001; Piro et al. 2002; Jakobsson et al. 2005; Castro-Tirado et al. 2007b; Rol et al. 2007; Berger et al. 2007; Zauderer & Berger 2011). The X-Ray Telescope (XRT, Burrows et al. 2005) onboard *Swift* (Gehrels et al. 2004) provides these positions (accuracy of $\lesssim 2''.0$, Goad et al. 2007; Butler 2007) for the first time with large number statistics (~ 100 events per year), facilitating the build-up of large, well-defined samples of GRBs, afterglows and hosts with minimal optical biases (Hjorth et al. 2012).

GRB host spectroscopy is however mostly performed with optical spectrographs (Savaglio et al. 2009; Levesque et al. 2010). This gives rise to a redshift desert ($1.4 \lesssim z \lesssim 2.5$) where the strongest recombination and forbidden lines are outside the optical wavelength range. Spectroscopic studies of GRB hosts were thus limited to the low-redshift end of the GRB redshift distribution until NIR spectroscopy became feasible (Krühler et al. 2012; Chen 2012).

[†] Based on observations collected at the European Southern Observatory, Paranal, Chile, Program IDs: 177.A-0591, 080.A-0825, 084.A-0303, 086.B-0954, 087.B-0737, 088.A-0644.

¹ Dark Cosmology Centre, Niels Bohr Institute, University of Copenhagen, Juliane Maries Vej 30, 2100 Copenhagen, Denmark.

² Centre for Astrophysics and Cosmology, Science Institute, University of Iceland, Dunhagi 5, 107 Reykjavik, Iceland

³ Department of Physics, University of Warwick, Coventry CV4 7AL, UK

⁴ Department of Physics and Astronomy, University of Leicester, University Road, Leicester, LE1 7RH, UK

⁶ <http://www.mpe.mpg.de/~jcg/grbgen.html>

⁷ <http://www.raunvis.hi.is/~pja/GRBsample.html>

⁸ <http://www.grbhosts.org>

Here we present simultaneous optical/NIR spectroscopy with VLT/X-shooter for 19 *Swift* GRB hosts galaxies with the aim of increasing the redshift completeness of The Optically Unbiased GRB Host (TOUGH⁹, Hjorth et al. 2012; Malesani et al. 2012; Jakobsson et al. 2012; Milvang-Jensen et al. 2012; Michałowski et al. 2012 and this work) survey. Our observations provide accurate redshifts for 13 *Swift* GRBs, out of which nine GRBs are characterized as dark, i.e., with suppressed afterglow flux in the optical wavelength range as compared to the X-ray regime. We use our new redshift determinations to illustrate the bias in previous GRB samples primarily based on afterglow spectroscopy.

2. OBSERVATIONS AND DATA REDUCTION

2.1. Sample Selection

The GRB hosts in this work have been selected from two sources (Table 1). The bulk of the sample was taken from the TOUGH survey, while the remaining hosts were specifically chosen because of the dark nature of their afterglows. Dark GRBs were selected because they were localized to sub-arcsecond accuracy, either from *Chandra* X-ray or NIR ground-based afterglow observations, yielding reliable host associations.

Furthermore, we required that the hosts had existing imaging for a precise slit-alignment. Pre-imaging has been obtained with VLT FORS2 or ISAAC (Malesani et al. 2012) and HST ACS or WFC3 (Perley et al. 2012). Finding charts centered on the respective hosts are shown in Figures 1 and 2. The four galaxies not part of TOUGH (GRBs 071021, 080207, 090113, 090407) have brightnesses¹⁰ between $F606W > 27$ mag and $R \sim 24.5$ mag and $K \sim 21$ mag to $K \sim 19.5$ mag, making them comparatively red and NIR bright. The brightness of the TOUGH hosts in this paper is in the range $26.5 \text{ mag} \geq R \geq 22.9 \text{ mag}$ ($K \geq 20.0 \text{ mag}$).

2.2. X-shooter Observations

We observed the hosts spectroscopically with the VLT equipped with X-shooter (Vernet et al. 2011). X-shooter is a medium resolution, cross-dispersed, echelle spectrograph capable of obtaining simultaneous spectra from 3000 to 25 000 Å in three arms (ultra-violet/blue (UVB), visual (VIS) and NIR arm).

Our hosts were observed in nodding mode, with effective integration times ranging from 0.4 to 2.0 hr. Slit widths of the different arms were typically chosen to be 1''.0 (UVB) and 0''.9 (VIS and NIR). This results in approximate resolving powers $\lambda/\Delta\lambda \approx 5100, 8800, 5300$ for the UVB, VIS, and NIR arm, respectively. Details about our X-shooter observations can be found in Table 1.

2.3. Data Reduction

X-shooter data were reduced with the ESO/X-shooter pipeline v. 1.3.7 (Goldoni et al. 2006). The wavelength solution was obtained against arc-lamp frames, leaving residuals with an RMS of better than 0.3 pixels in all cases ($\approx 7.5 \text{ km s}^{-1}$ at $1.2 \mu\text{m}$). A cross-calibration of all individual NIR spectra using sky-lines provided consistent results. Robust absolute flux measurements in the broad wavelength range of X-shooter are challenging. They are most reliably

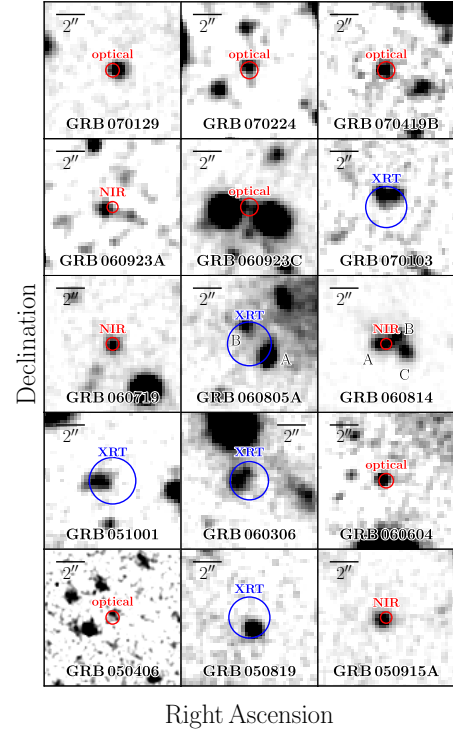


Fig. 1.— VLT/FORS *R*-band finding charts ($10'' \times 10''$) for our 15 TOUGH GRBs where North is up and East is left in all panels. Afterglow positions (ground-based optical/NIR or *Swift*/XRT X-ray) are indicated by red and blue circles. Photometry, positions and errors are described in detail in Malesani et al. (2012). Images are smoothed and the radii of optical/NIR error circles are indicative to enhance clarity. In cases where more than one galaxy is detected in the vicinity of the respective error-circles, the most likely host is labeled with A.

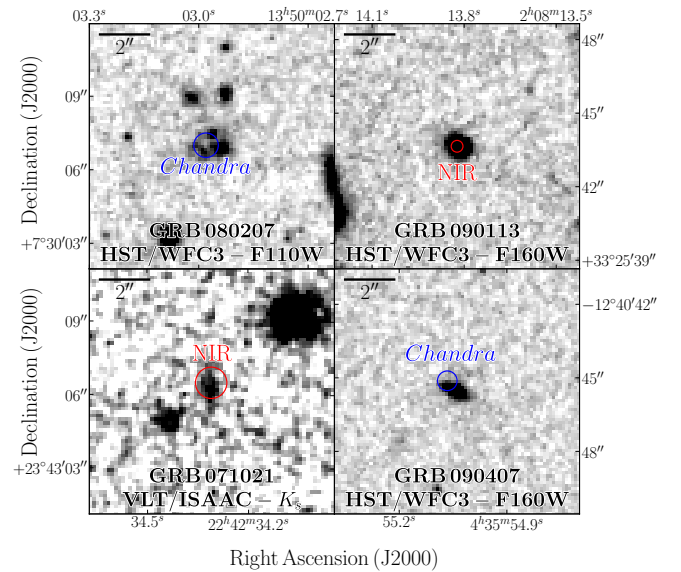


Fig. 2.— Finding charts ($10'' \times 10''$) for the four non-TOUGH GRBs 071021, 080207, 090113, and 090407 where North is up and East is left in all panels. Afterglow positions (ground-based NIR or *Chandra* X-ray) are indicated by red and blue circles. Photometry, positions and errors are described in detail in Perley et al. (2012).

⁹<http://www.dark-cosmology.dk/TOUGH>

¹⁰All magnitudes in this work are given in the Vega system.

TABLE 1
DETAILS OF GRB HOST SELECTION, OBSERVATIONS AND REDSHIFTS

GRB/Host	$\beta_{\text{OX}}^{(a)}$	Brightness R -band (mag)	$p_{\text{chance}}^{(b)}$	Exposure time (s)		Airmass	Seeing ($''$)	Selection ^(c,d)	Emission Lines ^(h)	Redshift
				UVB/VIS	NIR					
050406 ^(c)	1.0	26.6	0.02	3×1800	6×900	1.3	0 $''$.8	TOUGH
050819 ^(c)	< 0.9	24.1	0.03	2×900	4×450	1.7	0 $''$.7	TOUGH	([O II], H β), [O III]	2.5043 ± 0.0007
050915A ^(c,d)	< 0.4	24.6	0.004	6×1200	12×600	1.3	0 $''$.8	TOUGH	[O II], H β , ([O III])	2.5273 ± 0.0003
051001 ^(c,d)	< 0.6	24.4	0.05	2×1800	4×900	1.1	0 $''$.7	TOUGH	H β , [O III], (H α)	2.4296 ± 0.0003
060306 ^(c,d)	< 0.5	24.1	0.03	$2 \times 900/2 \times 938$	$2 \times 2 \times 490$	1.2	1 $''$.9	TOUGH
060604 ^(c)	0.8	25.5	0.01	4×1800	8×900	1.1	0 $''$.8	TOUGH	H β , [O III], H α	2.1357 ± 0.0002
060719 ^(c,d)	< -0.1	24.6	0.005	4×1500	12×500	1.2	0 $''$.7	TOUGH	([O II]), H α	1.5320 ± 0.0004
060805A ^(c,d)	< 1.1	23.5	0.02	4×1200	12×420	1.4	2 $''$.0	TOUGH
060814 ^(c,d)	< -0.1	22.9	0.002	2×1800	$2 \times 3 \times 600$	1.5	0 $''$.8	TOUGH	[O II], [O III], H α	1.9229 ± 0.0004
060923A ^(c,d,e)	< 0.1	26.1	0.02	6×1200	12×600	1.3	1 $''$.0	TOUGH
060923C ^(c,d)	< 0.3	25.5	0.02	$2 \times 730/2 \times 680$	6×270	1.3	0 $''$.7	TOUGH
070103 ^(c,d)	< 0.5	24.2	0.04	2×900	4×450	1.7	0 $''$.8	TOUGH	(H β), [O III]	2.6208 ± 0.0007
070129 ^(c,d)	0.6	24.4	0.004	4×900	$4 \times 3 \times 300$	1.7	1 $''$.4	TOUGH	[O II], [O III], H α	2.3384 ± 0.0003
070224 ^(c)	0.9	26.0	0.15	6×1200	12×600	1.1	0 $''$.5	TOUGH
070419B ^(c,d)	0.3	25.2	0.01	6×1200	12×600	1.1	1 $''$.1	TOUGH	[O III], H α	1.9588 ± 0.0003
071021 ^(f)	< 0.4	$V = 25.3^{(f)}$	0.007	2×1200	4×600	1.6	0 $''$.9	dark	H β , [O III], H α	2.4520 ± 0.0004
080207 ^(f)	< 0.3	$25.8^{(c,g)}$	0.01	6×1200	$4 \times 3 \times 600$	1.2	0 $''$.9	dark	[O III], H α	2.0858 ± 0.0003
090113 ^(f)	< 0.3	$V = 24.6^{(f)}$	0.005	2×1800	4×900	2.0	0 $''$.7	dark	[O II], H α	1.7493 ± 0.0002
090407 ^(f)	< 0.4	$F606W > 27^{(f)}$	0.02	2×1800	4×900	1.0	0 $''$.6	dark	[O II], (H β), H α	1.4485 ± 0.0006

NOTE. — ^(a) Optical-to-X-ray spectral index from Fynbo et al. (2009b) for TOUGH events. Afterglows with $\beta_{\text{OX}} < 0.5$ are defined as dark by Jakobsson et al. (2004). ^(b) Estimated chance probability of finding an unrelated galaxy along the line of sight to the GRB. ^(c) The TOUGH sample and photometry is described in Hjorth et al. (2012) and Malesani et al. (2012). ^(d) TOUGH VLT/FORS spectroscopy in Jakobsson et al. (2012). ^(e) Tanvir et al. (2008). ^(f) Perley et al. (2012). ^(g) Rossi et al. (2012). ^(h) Line transitions in the X-shooter spectrum. Values in round parentheses denote tentative detections, i.e., significant below 3σ or strongly affected by sky-line contamination. The horizontal line separates the objects in the TOUGH sample from four extra systems that were observed within our program.

performed by scaling the spectral continuum to broad-band imaging within a similar wavelength interval. As for most of our targets both the necessary imaging as well as the detection of the host continuum are absent, we defer any analysis beyond line identification and redshift determination to forthcoming works.

3. RESULTS AND DISCUSSION

3.1. Selection Effects

In principle, X-shooter is capable of measuring redshifts via strong recombination or forbidden lines up to $z \sim 5$, which is when [O II]($\lambda\lambda$ 3726, 3729) is redshifted out of the NIR range. However, several selection effects play an important role in the redshift distribution of our sample.

Firstly, the target selection is primarily based on host imaging within the TOUGH survey, yielding brightnesses between $26.5 \text{ mag} \geq R \geq 23 \text{ mag}$, which biases the redshift distribution towards low-redshift events. This bias is evident, for example, from the distribution of host magnitudes for which a redshift is available via afterglow spectroscopy (see e.g., Fig. 11 in Hjorth et al. 2012). GRB hosts at $z > 3$ are typically fainter than the sensitivity limit of the TOUGH survey ($R \sim 27 \text{ mag}$). Similarly, the targeted X-shooter hosts of this work are on average fainter and at higher redshifts than, for example, the hosts of the FORS campaign (Jakobsson et al. 2012). Overall, the TOUGH survey shows an obvious trend of a decreasing median apparent brightness with increasing redshift for GRB hosts (see e.g., Fig. 8 in Hjorth et al. 2012).

Secondly, most of the hosts were already observed with optical spectrographs (Jakobsson et al. 2012). Only if the optical spectroscopy did not reveal emission lines were the hosts further targeted with X-shooter. As a result of these selection criteria we expect our galaxies to be located in or above the redshift desert ($1.4 < z \lesssim 3$). In addition, there are further redshift ranges where emission lines are located in regions of low

sky transparency making redshift measurements challenging observationally for example between $2.7 \lesssim z \lesssim 2.9$. Above $z = 2.9$, all lines except [O II] are located in the K -band, where the thermal background of X-shooter is high.

3.2. Host Associations

GRB redshifts from their putative host galaxies always rely on the probabilistic association between galaxy and GRB event. Typical probabilities of associating an unrelated galaxy with the GRB (p_{chance}) being in the 1-5% range for $2''$ -0-sized error-boxes and galaxies with brightnesses of around $R \sim 25 \text{ mag}$ (Perley et al. 2009).

For 14 events in our sample, the association between GRBs and galaxy is unambiguous because of accurate afterglow positions from optical/NIR (typical accuracy $\lesssim 0''.3$) or dedicated *Chandra* X-ray (typical accuracy $\sim 0''.5$) imaging (Figures 1 and 2). Only in five cases does the association rely on a *Swift*/XRT position (typical accuracy $\sim 1''.5$).

Using the magnitudes from the TOUGH survey and Perley et al. (2012), we derive probabilities of associating an unrelated galaxy along the line of sight to the GRB (see Table 1) following Bloom et al. (2002). These chance probabilities are $p_{\text{chance}} \lesssim 0.15$ for all our events, or $p_{\text{chance}} \lesssim 0.05$ for those with redshifts. We caution, that these values are strictly valid only for single events, and if the individual GRB sight-line probes a random line of sight through the Universe (see e.g., Bloom et al. 2002; Perley et al. 2009, for a detailed discussion). Further support to the host assignments is added in the case where redshift determinations were successful: our redshift measurement depends on nebular and forbidden lines and thus star-formation, which is closely related to GRB formation. Together with the small chance probabilities, we hence consider the physical association between GRB and galaxy, and thus redshift, robust.

3.3. Emission Lines and Redshifts

Our X-shooter spectroscopy provides accurate redshifts for 13 of the 19 targeted galaxies. Figure 3 summarizes the detection of different recombination or forbidden lines and Table 1 shows the respective line transitions and redshifts. For eleven galaxies, two or more emission lines are detected at high significance yielding a robust and unique redshift. For two host galaxies (GRBs 050819 and 060719) only one line is detected at $S/N > 3$, and the line identification is thus not immediately clear. These are discussed in Sections 3.3.1 and 3.3.3.

The median redshift is $\bar{z} = 2.1$ for all the 13 galaxies or $\bar{z} = 2.3$ for the nine TOUGH hosts (Table 1) with accurate X-shooter emission line redshifts. Due to our initial selection and the unique NIR sensitivity of X-shooter, this is much higher than the median redshift of hosts ($\bar{z} = 0.7$) for which host spectroscopy has been published before the TOUGH survey (Figure 4). Our targets were furthermore chosen to maximize the success rate of a redshift determination, and are thus skewed to the lower redshift end of the distribution of TOUGH GRBs with unknown redshift (Hjorth et al. 2012).

The median (mean) R -band brightness of the galaxies with successful redshift measurement is $\bar{R} = 24.6$ mag (mean $\langle R \rangle \sim 24.8$ mag). The galaxies for which we could not obtain redshifts with our X-shooter spectroscopy were either observed under unfavorable sky conditions (GRBs 060306 and 060805A, see Table 1) or significantly fainter ($\bar{R} = 26.0$ mag, GRBs 050406, 060923A, 060923C, 070224) than the ones with redshift measurements. They are thus likely located at an even higher redshift than $\bar{z} = 2.1$ on average (see Section 3.1 and also Hjorth et al. 2012).

For GRB hosts above $z \gtrsim 1.6$, the redshifted, resonant $\text{Ly}\alpha$ transition is within the spectral response of X-shooter. However, we do not detect significant $\text{Ly}\alpha$ emission in any of the 17 X-shooter spectra (after excluding those hosts where $\text{Ly}\alpha$ is securely out of the X-shooter band-pass). This is due to a combination of several effects: 13 out of 17 GRBs had no detection of an optical afterglow, and 10 out of the 17 were firmly dark (and thus dusty). Dust plays a crucial role in the escape fraction of $\text{Ly}\alpha$ photons, and the strength of the $\text{Ly}\alpha$ line (Fynbo et al. 2003; Milvang-Jensen et al. 2012). In addition also the insignificant depth of our observations (e.g., GRBs 060306 and 060805A) as well as galaxy faintness (e.g., GRBs 050406, 070224) contribute to the $\text{Ly}\alpha$ non-detection.

But even for hosts with a bright optical afterglow (indicative of little dust along the GRB sight line), vigorous star formation, and an appropriate redshift, such as the galaxies hosting GRBs 060604 and 070129, $\text{Ly}\alpha$ emission is not ubiquitous (see also Figure 11 of Milvang-Jensen et al. 2012). This could be indicative of a heterogeneous distribution of dust in the inter-stellar medium of the hosts, as the afterglow probes only a specific sight-line, while the $\text{Ly}\alpha$ emission is an integrated property of the galaxy. A quantitative and more in depth discussion of the $\text{Ly}\alpha$ properties of our sample is beyond the scope of this paper and deferred to a future work.

For the six GRBs 050406, 060306, 060805A, 060923A, 060923C and 070224 no emission lines were detected, and our observations hence do not provide an accurate redshift. Based on the detection of the host galaxy in the FORS/ R -band (Figure 1 and Malesani et al. 2012), the redshift of these six GRBs is constrained to $z < 5$. The detection of the afterglow of GRB 050406 in the UVOT/ u -band limits its redshift further to $z \lesssim 3.2$ with a proposed photo- z of $z \sim 2.4$ by Schady et al. (2006). Additional redshift constraints based on the detection

of continuum emission in low-resolution host spectroscopy are $z \lesssim 2.8$ for GRB 060923A (Tanvir et al. 2008) and $z \lesssim 2.5$ for GRB 060805A and GRB 060306 (Jakobsson et al. 2012).

3.3.1. GRB 050819

A bright emission line is detected in the X-shooter spectrum of GRB 050819 at a wavelength of 17545 \AA , which could be interpreted as [O II] at $z = 3.71$, [O III]($\lambda 5007$) at $z = 2.504$ or $\text{H}\alpha$ at $z = 1.673$. In the case of [O II], we would expect to resolve the doublet of [O II]($\lambda\lambda 3726, 3729$) with two components of comparable intensity separated by 14 \AA . If the line was $\text{H}\alpha$, then [O III]($\lambda 5007$) and/or [O II] should be detected for typical line ratios. Hence, we interpret the line as [O III]($\lambda 5007$) at $z = 2.504$. The marginal flux seen at the expected positions of [O II] and $\text{H}\beta$ at $z = 2.504$ with $S/N \lesssim 2$ (Figure 3) further supports our association. $\text{H}\alpha$ at $z = 2.504$ is redshifted to $\lambda_{\text{obs}} = 22998 \text{ \AA}$ and our non-detection of $\text{H}\alpha$ is caused by the increased thermal background of X-shooter in this wavelength regime.

3.3.2. GRB 060306

A redshift of $z = 3.5$ for GRB 060306 based on the detection of a single emission line interpreted as [O II] via X-shooter spectroscopy was reported by Salvaterra et al. (2012). Our X-shooter data are too shallow to confirm or reject the line detection. Photometric and spectroscopic observations, however, indicate a lower redshift solution with $z \lesssim 2.5$ (Jakobsson et al. 2012). We therefore consider an association of the line with [O III]($\lambda 5007$) at $z = 2.35$ or $\text{H}\alpha$ at $z = 1.55$ more plausible.

3.3.3. GRB 060719

We detect a single, bright emission line at 16616 \AA in the X-shooter spectrum of the dark GRB 060719 ($\beta_{\text{OX}} < -0.1$). [O II] is readily excluded as the line is not resolved into two components. Using the redshift constraint ($z < 2.0$) from the host continuum emission (Jakobsson et al. 2012), we interpret this line as $\text{H}\alpha$ at $z = 1.532$. The flux increase seen at the corresponding wavelength of [O II] ($\lambda_{\text{obs}} = 9440 \text{ \AA}$) strongly supports this interpretation. [O III]($\lambda 5007$) at $z = 1.532$ is located at $\lambda_{\text{obs}} = 12677 \text{ \AA}$, a region dominated by bright sky-lines. We hence consider the redshift robust.

3.3.4. GRB 060814

A redshift of $z = 1.92$ for the dark GRB 060814 ($\beta_{\text{OX}} < -0.1$) based on these data was reported by Salvaterra et al. (2012). The system hosting GRB 060814 consists of two galaxies A and B separated by $1''.3$ (Figure 1 and Jakobsson et al. 2012) at redshifts of $z_A = 1.923$ and $z_B = 1.920$. The location of the NIR afterglow is consistent with galaxy A, and $z_A = 1.923$ is the redshift of GRB 060814. Galaxy C from Figure 1 is an unrelated foreground object.

3.3.5. GRBs 050915A, 051001, 060604, 070103, 070129 and 070419B

These six hosts from the TOUGH sample have at least two emission lines detected at high significance (Figure 3). The redshift of the galaxies is hence uniquely determined, and the redshift of the GRB only relies on the association between burst and galaxy (Malesani et al. 2012). This association is very robust for GRBs 050915A, 060604, 070129 and 070419B because of an accurate position from an optical/NIR

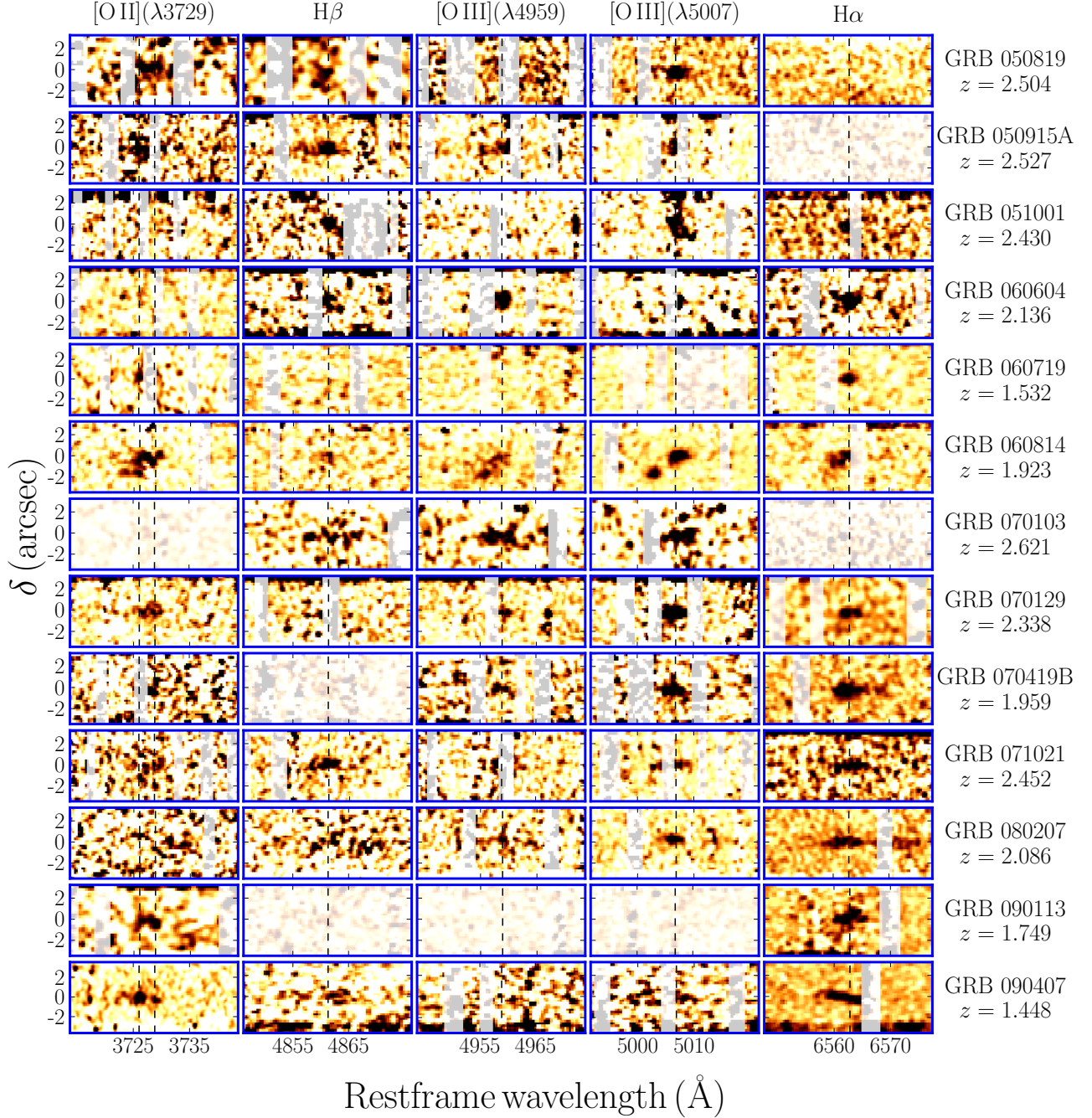


FIG. 3.— Two-dimensional cutouts of 13 X-shooter spectra used for redshift determination. Each column is centered at the rest-frame wavelength of a strong emission line, marked by vertical dashed lines. Regions of sky-lines and negligible sky or X-shooter transmission are indicated with grey shading.

afterglow (Figure 1). Only for GRBs 051001 and 070103 is it based on the *Swift*/XRT position with uncertainties of $1''.7$ and $1''.5$ at 90% confidence (Figure 1). The corresponding redshifts are provided in Table 1 and Figure 3.

3.3.6. GRB 071021

The afterglow of the dark ($\beta_{\text{OX}} \lesssim 0.4$) GRB 071021 was detected as a fading source in the NIR only (Castro-Tirado et al. 2007a). The galaxy at a position consistent with the afterglow (Figure 2) has a redshift of $z = 2.452$ based on the detection of the emission lines of $\text{H}\beta$, $[\text{O III}]$, and $\text{H}\alpha$ (Figure 3). Our spectroscopic redshift rules out a high-redshift nature for this event, and the red color of the afterglow is attributed to ex-

tinction by dust in the ISM of the host.

3.3.7. GRB 080207

The luminous and massive host of the dark ($\beta_{\text{OX}} \lesssim 0.3$) GRB 080207 was studied in detail photometrically by Hunt et al. (2011) and Svensson et al. (2012), yielding photometric redshifts of $z^{\text{phot}} \sim 2$. The spectroscopic redshift based on $\text{H}\alpha$ and $[\text{O III}]$ is $z^{\text{spec}} = 2.086$, and thus confirms the estimation by the preceding authors.

3.3.8. GRB 090113

The optical afterglow of the dark GRB 090113 was not detected in NOT *R*-band imaging (de Ugarte Postigo et al.

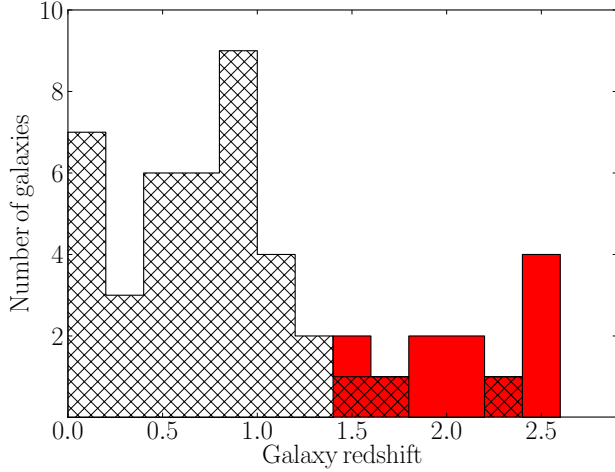


FIG. 4.— Histogram of GRB host redshifts with published spectroscopy. Hatched data were taken from the literature (Savaglio et al. 2009, including updates from <http://www.grbhosts.org>), red from this work.

2009b), which yields $\beta_{\text{OX}} \lesssim 0.3$. The galaxy associated with the burst via a NIR afterglow position (Figure 2, A. J. Levan, priv. communication) has a redshift of $z = 1.749$ based on the detection of the emission lines of [O II] and H α (Figure 3). At this redshift, H β and [O III] are located in regions of limited atmospheric transmission.

3.3.9. GRB 090407

The afterglow of the dark GRB 090407 was not detected in deep VLT/FORS or GROND optical/NIR imaging (Malesani & Fynbo 2009; Afonso et al. 2009), implying $\beta_{\text{OX}} \lesssim 0.4$. The galaxy associated with GRB 090407 via *Chandra* observations (Figure 2, A. J. Levan, priv. communication) has a redshift of $z = 1.448$, which relies on the detection of [O II] and H α (Figure 3). At this redshift, H β and [O III] are located in a region dominated by bright sky-lines.

3.4. Absorption Properties of dark GRBs

Having an accurate redshift measurement enables quantitative studies of the material along the line of sight. Low-energy X-ray afterglow photons are, for example, absorbed by intervening metals. This metal column density is typically converted into an equivalent hydrogen column at the redshift of the GRB assuming solar metallicity $N_{\text{H,X}}$. The inferred $N_{\text{H,X}}$ values are generally much higher than the neutral hydrogen column density measured from GRB DLAs, and the exact physical nature and location of the material causing the soft X-ray absorption excess is currently not fully understood (e.g., Schady et al. 2011; Watson & Jakobsson 2012).

Figure 5 shows the probability density function and cumulative distribution of $N_{\text{H,X}}$ at the burst's redshift for dark GRBs with $\beta_{\text{OX}} < 0.5$ and an accurate redshift. We selected the dark GRBs from this work as well as several events from the literature (Greiner et al. 2011; Krühler et al. 2011b; Perley et al. 2012). X-ray data for all events were taken from the *Swift*-XRT online repository (Evans et al. 2007, 2009) and analyzed in standard manner in XSPEC12 using abundances from Anders & Grevesse (1989). The selected bursts, their redshifts, and $N_{\text{H,X}}$ values are given in Table 2. As a comparison sample, we used 79 optically-bright, redshift-selected *Swift* GRBs and their $N_{\text{H,X}}$ values up to June 2009 from Table 1 in Campana et al. (2010).

TABLE 2
 $N_{\text{H,X}}$ VALUES FOR THE DARK GRBs WITH SPECTROSCOPIC REDSHIFTS

GRB	Redshift	β_{OX}	$N_{\text{H,X}}$ (10^{22} cm^{-2})	References
050915A	2.53	< 0.4	$1.1^{+0.7}_{-0.6}$	(1, 2)
060210	3.91	0.4	2.4 ± 0.4	(2)
060719	1.53	< -0.1	$1.9^{+0.5}_{-0.4}$	(1, 2)
060814	1.92	< -0.1	$3.4^{+0.3}_{-0.4}$	(1, 2)
061222A	2.09	< 0.2	3.7 ± 0.4	(2)
070103	2.62	< 0.5	$4.1^{+1.3}_{-1.1}$	(1)
070306	1.50	< 0.2	2.5 ± 0.3	(2)
070419B	1.96	0.3	0.8 ± 0.2	(1)
070521	1.35	< -0.1	4.8 ± 0.7	(2)
070802	2.45	0.5	$0.8^{+0.8}_{-0.6}$	(2, 3)
071021	2.45	< 0.4	1.3 ± 0.4	(1)
080207	2.09	< 0.3	$15.1^{+2.3}_{-2.2}$	(1)
080805	1.50	0.4	$1.2^{+0.7}_{-0.5}$	(2, 3)
080913	6.7	< 0.1	$0.4^{+6.2}_{-0.4}$	(2, 3)
081109	0.98	< 0.4	0.9 ± 0.2	(3, 4)
081221	2.26	< 0.2	4.6 ± 0.6	(5)
090102	1.55	0.5	$0.7^{+0.2}_{-0.1}$	(3, 6)
090113	1.75	< 0.3	$2.0^{+0.8}_{-0.6}$	(1)
090407	1.45	< 0.4	1.8 ± 0.3	(1)
090812	2.45	0.5	0.6 ± 0.4	(3, 7)
090926B	1.24	0.4	$1.4^{+0.5}_{-0.4}$	(3, 8)
100621A	0.54	0.4	1.9 ± 0.2	(4, 9)

NOTE. — References: (1) This work, (2) Fynbo et al. (2009b), (3) Greiner et al. (2011), (4) Krühler et al. (2011b), (5) Salvaterra et al. (2012), (6) de Ugarte Postigo et al. (2009c), (7) de Ugarte Postigo et al. (2009a), (8) Fynbo et al. (2009a), (9) Milvang-Jensen et al. (2010)

The median (mean) X-ray column densities $\log(N_{\text{H,X}})$ for both distributions are $\log(N_{\text{H,X}}/\text{cm}^{-2}) = 21.8$ (21.8) for the optically bright and $\log(N_{\text{H,X}}/\text{cm}^{-2}) = 22.3$ (22.2) for the dark *Swift* events. Clearly, dark (which are predominantly dusty) bursts have significantly higher $N_{\text{H,X}}$ values with its most extreme example GRB 080207 exceeding $N_{\text{H,X}} > 10^{23} \text{ cm}^{-2}$ (Figure 5). The K.-S.-test p -value is 2.3×10^{-4} and the null-hypothesis, that both distributions are drawn from the same parent distribution, can hence be rejected at 3.7σ confidence in a normal probability distribution.

This result is not unexpected. Per selection, we have compared dark bursts which are predominantly dusty (with a few high-redshift interlopers) against dust-poor sight-lines, and metals are a prerequisite of forming dust. There is hence a tight connection between the darkness of the afterglow and the soft X-ray absorption. It furthermore illustrates how our understanding of GRB and host galaxy properties is limited by the effect of incompleteness in redshift samples (see also Fynbo et al. 2009b; Campana et al. 2012), and how X-shooter spectroscopy of GRB hosts is capable of efficiently removing this bias.

4. CONCLUSIONS

We have presented optical/NIR spectroscopy of a sample of 19 *Swift* GRBs primarily taken from the TOUGH survey. In total, we measure 13 redshifts, including the redshifts of nine dark GRBs. The median redshift of these 13 galaxies is $\bar{z} = 2.1$, and it is $\bar{z} = 2.3$ for our nine bursts from the TOUGH survey. This establishes NIR host spectroscopy as an efficient tool for redshift determination in the redshift desert at $z \gtrsim 1.4$ (Figure 4) and in those cases where optical/NIR afterglow absorption line spectroscopy is not successful.

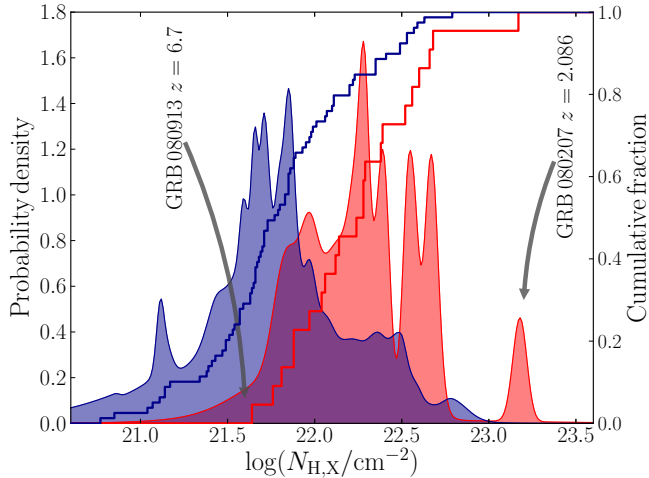


Fig. 5.— Normalized probability density function and cumulative distribution of soft X-ray absorption at the burst's redshift for 79 optically-bright *Swift* GRBs in blue (Campana et al. 2010) and 22 dark GRBs in red with spectroscopic redshifts (Table 2). The probability density function (PDF) is derived by assuming continuous normal distributions of $N_{\text{H,X}}$ for single GRBs with asymmetric width set by the measured uncertainties (see e.g., Evans et al. 2009). The plotted PDF is then the sum over the individual distributions of $N_{\text{H,X}}$ normalized to the number of GRBs. The location of the high-redshift, dark GRB 080913 (Greiner et al. 2009) and the dusty, dark GRB 080207 are indicated in the plot.

X-shooter's sensitivity, resolution and wavelength coverage are ideally suited to perform redshift measurements for star-forming galaxies such as GRB hosts with brightnesses $R \sim 24.5$ mag and modest exposure times. Our observations yield redshifts for even fainter targets (GRBs 080207 with $R = 25.8 \pm 0.2$ mag or 090407 with $F606W > 27$ mag) in cases when the galaxies are NIR bright ($K \lesssim 21$ mag) and vigorously star forming.

In particular for highly-extinguished GRBs and afterglows, NIR host spectroscopy provides means to establish an accurate redshift, and thus lifts the bias in previous GRB samples, which typically lack redshift determinations for dark bursts.

This is a further step towards complete GRB samples, and hence a better understanding of the conditions in which GRBs form. A census of GRB hosts without physical selection biases is the key for measuring the fraction of star-formation that is traced by long GRBs. Samples like TOUGH are therefore of fundamental importance when using GRBs as tools to investigate galaxy evolution and star-formation in the early Universe.

T.K. acknowledges support from a Marie-Curie Intra-European Fellowship. D.M. acknowledges support from the Instrument Center for Danish Astrophysics. B.M.-J. and J.P.U.F acknowledge support from the ERC-StG grant EGG5-278202. P.J. acknowledges support by a Project Grant from the Icelandic Research Fund. The Dark Cosmology Centre is funded by the Danish National Research Foundation. We thank the referee for very valuable and constructive comments, G. Tagliaferri for imaging data of GRB 071021, G. Leloudas for comments on the manuscript, P. Vreeswijk for support and D. Perley for sharing his results before publication. This research has made use of the GHostS database (<http://www.grbhosts.org>), which is partly funded by Spitzer/NASA grant RSA Agreement No. 1287913. This work made use of data supplied by the UK *Swift* Science Data Centre at the University of Leicester.

Facilities: VLT:Kueyen (X-shooter), VLT:Antu (FORS2), VLT:Melipal (ISAAC), HST (WFC3)

REFERENCES

- Afonso, P., Olivares, F., Greiner, J., & Kruehler, T. 2009, GCN, 9109
 Anders, E., & Grevesse, N. 1989, *Geochim. Cosmochim. Acta*, 53, 197
 Berger, E., Fox, D. B., Kulkarni, S. R., Frail, D. A., & Djorgovski, S. G. 2007, *ApJ*, 660, 504
 Bloom, J. S., Kulkarni, S. R., & Djorgovski, S. G. 2002, *AJ*, 123, 1111
 Burrows, D. N., Hill, J. E., Nousek, J. A., et al. 2005, *SSR*, 120, 165
 Butler, N. R. 2007, *AJ*, 133, 1027
 Campana, S., Thöne, C. C., de Ugarte Postigo, A., et al. 2010, *MNRAS*, 402, 2429
 Campana, S., Salvaterra, R., Melandri, A., et al. 2012, *MNRAS*, 421, 1697
 Castro-Tirado, A. J., de Ugarte Postigo, A., Jelinek, M., et al. 2007a, GCN 6968, 6968
 Castro-Tirado, A. J., Bremer, M., McBreen, S., et al. 2007b, *A&A*, 475, 101
 Chen, H.-W. 2012, *MNRAS*, 419, 3039
 de Ugarte Postigo, A., Gorosabel, J., Fynbo, J. P. U., Wiersema, K., & Tanvir, N. 2009a, GCN, 9771
 de Ugarte Postigo, A., Gorosabel, J., Knapen, J. H., Sanchez Gallego, J. R., & Stiles, P. 2009b, GCN, 8810
 de Ugarte Postigo, A., Jakobsson, P., Malesani, D., et al. 2009c, GCN, 8766
 Djorgovski, S. G., Frail, D. A., Kulkarni, S. R., et al. 2001, *ApJ*, 562, 654
 Evans, P. A., Beardmore, A. P., Page, K. L., et al. 2007, *A&A*, 469, 379
 —. 2009, *MNRAS*, 397, 1177
 Fynbo, J. P. U., Malesani, D., Jakobsson, P., & D'Elia, V. 2009a, GCN, 9947
 Fynbo, J. P. U., Jakobsson, P., Möller, P., et al. 2003, *A&A*, 406, L63
 Fynbo, J. P. U., Jakobsson, P., Prochaska, J. X., et al. 2009b, *ApJS*, 185, 526
 Gehrels, N., Ramirez-Ruiz, E., & Fox, D. B. 2009, *ARA&A*, 47, 567
 Gehrels, N., Chincarini, G., Giommi, P., et al. 2004, *ApJ*, 611, 1005
 Goad, M. R., Tyler, L. G., Beardmore, A. P., et al. 2007, *A&A*, 476, 1401
 Goldoni, P., Royer, F., François, P., et al. 2006, in *SPIE Conf. Ser.*, Vol. 6269
 Greiner, J., Krühler, T., Fynbo, J. P. U., et al. 2009, *ApJ*, 693, 1610
 Greiner, J., Krühler, T., Klose, S., et al. 2011, *A&A*, 526, A30
 Groot, P. J., Galama, T. J., van Paradijs, J., et al. 1998, *ApJ*, 493, L27
 Hjorth, J., Malesani, D., Jakobsson, P., et al. 2012, *ApJ*, 756, 187
 Hunt, L., Palazzi, E., Rossi, A., et al. 2011, *ApJ*, 736, L36
 Jakobsson, P., Hjorth, J., Fynbo, J. P. U., et al. 2004, *ApJ*, 617, L21
 Jakobsson, P., Frail, D. A., Fox, D. B., et al. 2005, *ApJ*, 629, 45
 Jakobsson, P., Hjorth, J., Malesani, D., et al. 2012, *ApJ*, 752, 62
 Krühler, T., Fynbo, J. P. U., Geier, S., et al. 2012, *A&A*, in press, arXiv:1203.1919
 Krühler, T., Schady, P., Greiner, J., et al. 2011a, *A&A*, 526, A153
 Krühler, T., Greiner, J., Schady, P., et al. 2011b, *A&A*, 534, A108
 Levesque, E. M., Berger, E., Kewley, L. J., & Bagley, M. M. 2010, *AJ*, 139, 694
 Malesani, D., & Fynbo, J. P. U. 2009, GCN, 9108
 Malesani et al. 2012, in preparation
 Michałowski, M. J., Kamble, A., Hjorth, J., et al. 2012, *ApJ*, 755, 85
 Milvang-Jensen, B., Fynbo, J. P. U., Malesani, D., et al. 2012, *ApJ*, 756, 25
 Milvang-Jensen, B., Goldoni, P., Tanvir, N. R., et al. 2010, GCN, 876
 Perley, D. A., Cenko, S. B., Bloom, J. S., et al. 2009, *AJ*, 138, 1690
 Perley et al. 2012, in preparation
 Piran, T. 2004, *Reviews of Modern Physics*, 76, 1143
 Piro, L., Frail, D. A., Gorosabel, J., et al. 2002, *ApJ*, 577, 680
 Prochaska, J. X., Chen, H., & Bloom, J. S. 2006, *ApJ*, 648, 95
 Prochaska, J. X., Sheffer, Y., Perley, D. A., et al. 2009, *ApJ*, 691, L27
 Rol, E., van der Horst, A., Wiersema, K., et al. 2007, *ApJ*, 669, 1098
 Rossi, A., Klose, S., Ferrero, P., et al. 2012, *A&A*, in press, arXiv:1202.1434
 Salvaterra, R., Campana, S., Vergani, S. D., et al. 2012, *ApJ*, 749, 68
 Savaglio, S., Glazebrook, K., & Le Borgne, D. 2009, *ApJ*, 691, 182
 Schady, P., Savaglio, S., Krühler, T., Greiner, J., & Rau, A. 2011, *A&A*, 525, A113
 Schady, P., Mason, K. O., Osborne, J. P., et al. 2006, *ApJ*, 643, 276
 Svensson, K. M., Tanvir, N. R., Perley, D. A., et al. 2012, *MNRAS*, 421, 25
 Tanvir, N. R., Levan, A. J., Rol, E., et al. 2008, *MNRAS*, 388, 1743
 Vernet, J., Dekker, H., D'Odorico, S., et al. 2011, *A&A*, 536, A105
 Vreeswijk, P. M., Ledoux, C., Smette, A., et al. 2007, *A&A*, 468, 83
 Watson, D., & Jakobsson, P. 2012, *ApJ*, 754, 89
 Zafar, T., Watson, D., Fynbo, J. P. U., et al. 2011, *A&A*, 532, A143
 Zauderer, A., & Berger, E. 2011, GCN, 12190